ACS APPLIED NANO MATERIALS

www.acsanm.org Article

Highly Stable Core/Shell $AgIn_5S_8$/ZnS Quantum Dots for Pure White Light-Emitting Diodes

Yifang Sun, Liangliang Zhang, Ying Lv,* Qinghui Zeng,* Xiaoyang Guo, Wenyu Ji,* and Xingyuan Liu

Cite This: *ACS Appl. Nano Mater.* 2023, 6, 22311−22319 Read Online

ACCESS | Metrics & More | Article Recommendations | Supporting Information

ABSTRACT: $AgIn_5S_8$/ZnS (AIS/ZS) core/shell quantum dots (QDs) have been synthesized using a hot injection method at relatively low temperature without any protection using inert gas. The QDs were characterized with UV visible electronic absorption spectroscopy, PL spectroscopy, Fourier transform infrared (FT-IR) spectroscopy, transmission electron microscopy (TEM), and temperature-dependent time-resolved PL (TRPL). The average size of the QDs was determined to be 1.73 ± 0.29 nm. The QDs exhibit a major excitonic absorption band peaked at 479−573 nm and emission bands peaked from 548 to 666 nm with excitation at 410 nm with the peak position dependent on the synthesis temperature that affects the QD size. Upon the addition of trioctylphosphine (TOP) as a ligand, the PL quantum yield (PLQY) increased to 74.1% compared to 56.7% without TOP. The QDs show high stability after hours of ultraviolet (UV) light exposure or repetitive treatment with a significant amount of polar solvents, which is attributed to surface passivation by the ligands and ZnS shell. The luminescence mechanism of the core/shell AIS/ZS QDs is ascribed to donor−acceptor pair (DAP) recombination. TRPL results suggest that the binding energy of DAP increases and the DAP recombination probability is enhanced after passivation with TOP, leading to the high PLQY. Furthermore, prototype highly pure white light-emitting diodes (LEDs) based on these AIS/ZS QDs have been successfully demonstrated, yielding ideal 1931 CIE coordinates of (0.327, 0.335).

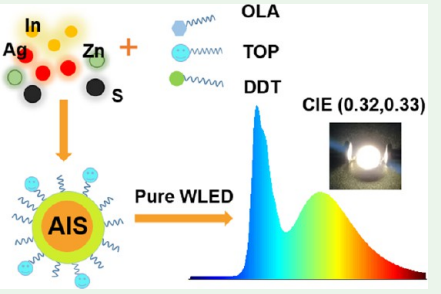

KEYWORDS: *AIS/ZS quantum dots, PLQY, high stability, white LED, DAP recombination*

1. INTRODUCTION

Semiconductor nanocrystals, also known as quantum dots (QDs), have garnered significant attention due to their unique optical, magnetic, and electrical properties arising from quantum confinement. They hold great promise for various applications such as light-emitting devices (LEDs), solar cells, and sensors.[1−7] Notably, QDs containing Cd and Pb elements have been comprehensively studied and extensively developed due to their high photoluminescence quantum yield (PLQY) and tunable emission ranging from ultraviolet (UV) to near-infrared (NIR) regions. Nevertheless, the inherent toxicity of heavy metals Cd and Pb raises concerns about health and environmental risks, which sternly restricts their practical application.[8−10] Therefore, the development and implementation of environmentally friendly QDs are highly desired.

Ternary I−III−VI QDs especially Ag−In−S (AIS) QDs have been studied as promising alternatives of traditional Cd-containing QDs due to their intrinsic low toxicity, large Stokes shift, wide excitation spectrum, and long fluorescence lifetime.[11−15] These unique optoelectronic properties of AIS QDs show promise for applications in LEDs, biomarkers, photovoltaics, and photocatalysis.[16−25] Different approaches have been developed to synthesize AIS QDs, including thermal decomposition methods,[26,27] high-temperature hot injection methods,[28] hydrothermal methods,[29] and microwave methods.[30] Dai et al. obtained AIS/ZS QDs with an enhanced PLQY of 70%[27] under 180 °C using the thermal decomposition method. Ma et al. prepared $AgInS_2$ QDs with a size between 3.5 and 4.4 nm and a PLQY of 8.8% by using microwave method.[30] Since the QDs tends to reactive and unstable to photon-irradiation,[31] a larger-band-gap (E_g) material, such as ZnS, is often used to create a shell around the AIS core for stabilization. Kwon et al. synthesized AgInZnS/CdS/ZnS QDs with a PLQY of 85.7% at 180 °C.[32] Chen et al. prepared AIS/ZS QDs with a PLQY of 45.7% by a hydrothermal method.[29] Current experimental processes necessitate high temperatures and long reaction times. Additionally, for LED and biological applications, QDs demand high photostability and surface stability. Hence, the design of a simpler synthesis process for producing efficient and highly stable AIS/ZS QDs is particularly crucial.

In this study, we synthesized AIS/ZS QDs by using a hot-injection method under low-temperature conditions without

Received: September 21, 2023
Revised: November 2, 2023
Accepted: November 3, 2023
Published: November 17, 2023

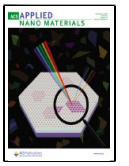

Scheme 1. Thermal Injection Process

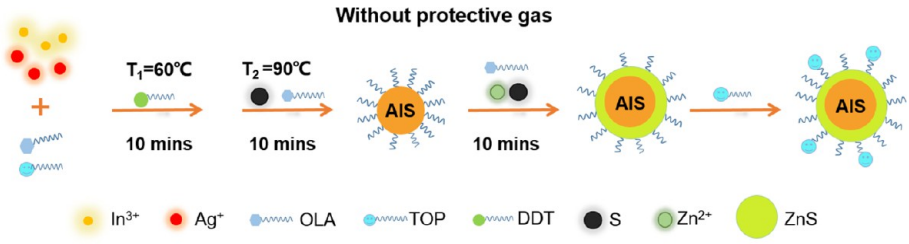

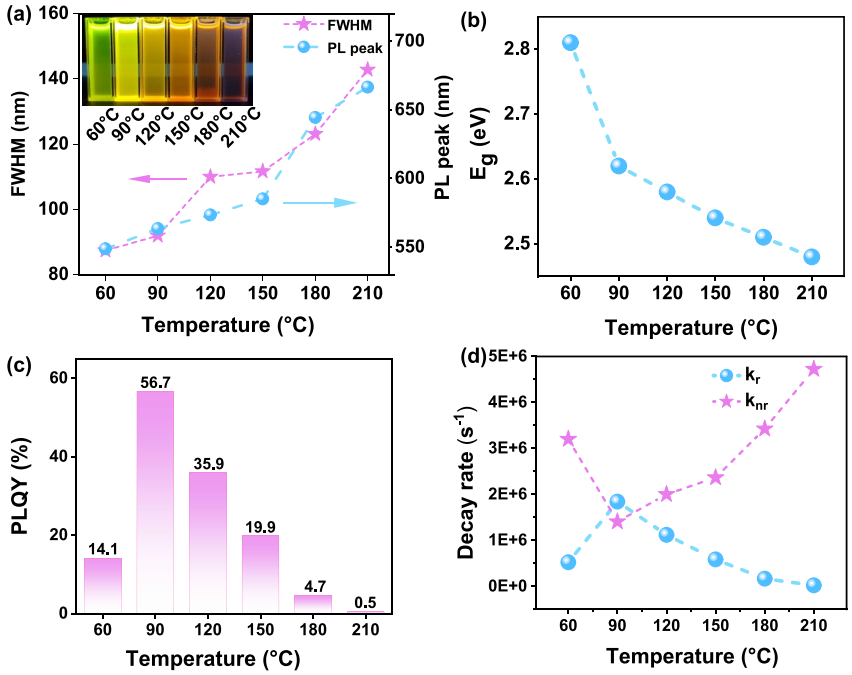

Figure 1. (a) PL emission peak and fwhm of AIS/ZS QDs with fluorescence photographs under UV irradiation (inset). (b) Optical band gap and (c) PLQY as a function of the synthesis temperature and (d) nonradiative recombination rate k_{nr} and radiative recombination rate k_r of AIS/ZS QDs as a function of S injection temperatures of 60, 90, 120, 150, 180, and 210 °C.

the need for inert gas protection. The average particle size of the QDs is 1.73 ± 0.29 nm. The QDs exhibit tunable absorption from 479 to 573 nm and PL emission from 548 to 666 nm. By systematically optimizing the reaction temperature and ligand (TOP), the maximum PLQY of these QDs was increased to 74.1%. Most importantly, the prepared AIS/ZS QDs possess excellent stability, including photostability, which is attributed to the surface passivation by the ligands. Furthermore, a pure white light-emitting diode based on these QDs was demonstrated.

2. RESULTS AND DISCUSSION

2.1. Optimization of Synthesis of AIS/ZS QDs by Varying Temperatures. Scheme 1 shows the schematic diagram of the synthesis process by using the hot-injection method. We injected ligand 1-dodecanethiol (DDT) in the mixture of Ag and In elements at 60 °C then injected a S source and raised it to the specified temperature. Finally, we introduced the shell material. The entire process does not require argon protection.

In the hot-injection method, the temperature is expected to play a pivotal role and significantly influences the size distribution, ligand attachment state, and luminescence properties of QDs. We systematically varied the temperature of the S source injection to optimize AIS/ZS QDs. Their UV−vis electronic absorption and PL spectra are shown in Figure S1. As the temperature increases, the excitonic absorption peak red shifts from 479.6 to 543.5 nm (Figure S2). Figure 1a shows the PL peak position and the full width at half-maximum (fwhm) with excitation at 410 nm as the reaction temperature increases from 60 to 210 °C; the PL emission peak red shifts from 548 to 666 nm accompanied by a broadening of the fwhm from 87 to 142 nm. The band gap E_g can be calculated using the relationship

$$\alpha_{h\upsilon} = (h\upsilon - E_g)^{1/2} \quad (1)$$

where α is the absorption coefficient and $h\upsilon$ is the photon energy. The calculated E_g values are plotted in Figure 1b. As the reaction temperature rises, the band gap undergoes a gradual decrease from 2.81 to 2.48 eV. Figure S3 shows the size distribution of QDs corresponding to different temperatures. With the increase of the temperature, the average size of QDs increases from 3.83 to 13.03 nm. We suggest that this is due to the nucleation process being temperature-sensitive. As the temperature increases, particles gradually grow larger, leading to larger QDs with redder absorption and emission as well as a broader PL band.[33]

https://doi.org/10.1021/acsanm.3c04490
ACS Appl. Nano Mater. 2023, 6, 22311−22319

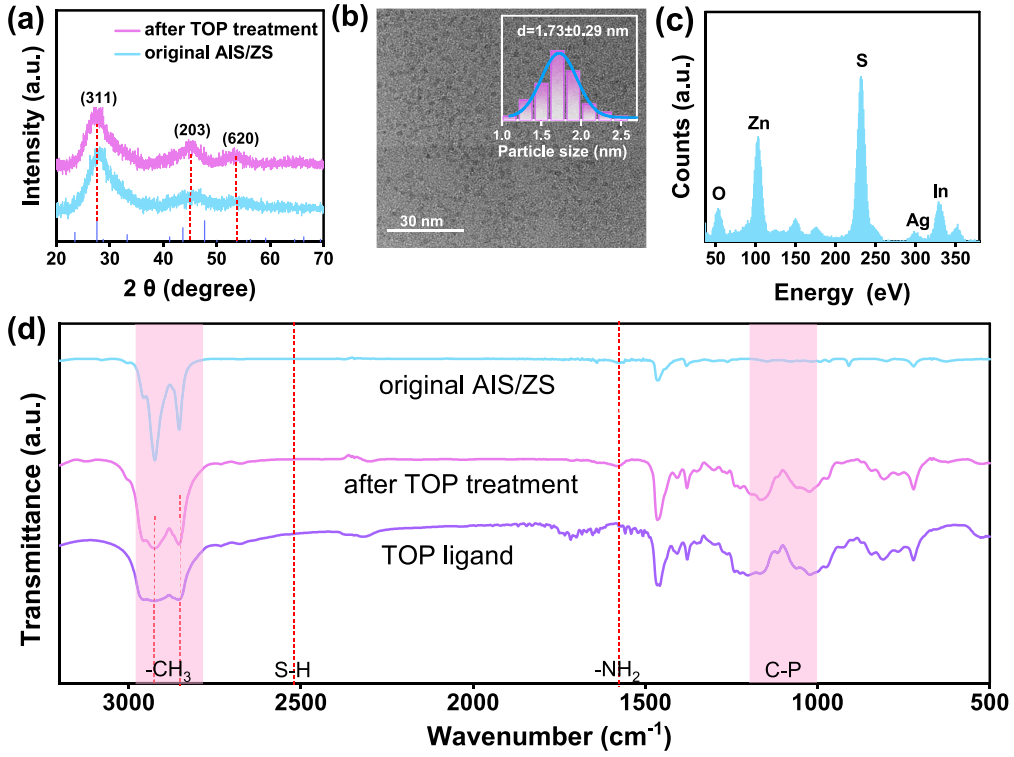

Figure 2. (a) XRD patterns of AIS/ZS QDs before and after the treatment with TOP. (b) TEM diagram of AIS/ZS QDs with the inset showing a particle size distribution and average size of 1.73 nm. (c) EDS spectrum of AIS/ZS QDs. (d) FT-IR spectra of original AIS/ZS QDs, QDs after TOP treatment, and the TOP ligand.

As shown in Figure 1c, the PLQY of AIS/ZS QDs increased from 14.1 to 56.7% as the temperature increased from 60 to 90 °C. However, further increasing the temperature to 120, 150, 180, and 210 °C resulted in a dramatic decrease in the PLQY, that is, only 0.5% at 210 °C. Based on the PLQY and observed fluorescence lifetime τ (Figure S4 and Table S1), we can calculate the nonradiative recombination rate k_{nr} and the radiative recombination rate k_r

$$\mathrm{PLQY} = \frac{k_r}{k_r + k_{nr}} \tag{2}$$

$$\tau = \frac{1}{k_r + k_{nr}} \tag{3}$$

then k_{nr} and k_r can be expressed as

$$k_{nr} = \frac{1 - \mathrm{PLQY}}{\tau} \tag{4}$$

$$k_r = \frac{\mathrm{PLQY}}{\tau} \tag{5}$$

The k_{nr} and k_r are shown in Table S2 and Figure 1d. As the temperature rises, k_r increases from 5.26×10^5 s^{-1} at 60 °C to 1.84×10^6 s^{-1} at 90 °C and decreases to 2.37×10^4 s^{-1} at 210 °C. The significantly increased radiative recombination rate and PLQY at 90 °C indicate that non-radiative recombination processes caused by processes such as surface defects are greatly suppressed at this temperature.[34] Meanwhile, too high of a temperature such as 210 °C here may cause the ligands to detach from the QD surface, leading to more surface defects, an increased k_{nr}, and a decreased PLQY.[35] Therefore, 90 °C was selected as the reaction temperature in this experiment.

2.2. Effect of the TOP ligand on AIS/ZS QDs. The XRD patterns of AIS/ZS QDs before and after treatment with TOP are shown in Figure 2a. We observed three broad peaks at 2θ = 27.3, 45.8, and 53.5°, which can be assigned to the (311), (203), and (620) planes of the cubic spinel $AgIn_5S_8$ (c-$AgIn_5S_8$) crystal, respectively.[36] Comparing the spectra, the position of the three broad peaks does not change, but the peak intensity increases after TOP treatment. This can be attributed to the increased crystallinity of AIS/ZS after the TOP treatment. TEM images in Figure 2b shows that the average particle size is 1.73 ± 0.29 nm (illustrated in Figure 2b) with a relative narrow distribution. The EDS energy spectrum of optimal AIS/ZS QDs is shown in Figure 2c, and the element ratio is shown in Table S3 in the Supporting Information. We find the molar ratio of Ag:In:S:Zn is 1:4.8:17.8:8.4, which basically matches the reaction feeding ratio Ag:In:S:Zn = 1:5:16:8. The content of S is slightly higher than the original ratio, which likely originates from the S provided by DDT after binding to the QD surface. Since EDS cannot accurately determine the P content, infrared spectroscopy was used to identify whether the TOP ligand was successfully attached to the surface of the AIS/ZS QDs.

Figure 2d shows the Fourier transform infrared (FT-IR) spectra of the original AIS/ZS QDs, QDs after TOP treatment, and TOP ligand. In the original preparation of AIS/ZS QDs, OLA and DDT ligands were added. The strong bands at 2921 and 2854 cm^{-1} are attributed to methyl-stretching patterns in DDT and OLA. Ligand amines bind to metal ion sites on the surface of QDs via lone pairs of electrons, and the peak at 1581 cm^{-1} can be attributed to the NH_2 shear pattern. Peaks in the frequency range below 1500 cm^{-1} are assigned to the C−H stretch vibration, C−C stretch vibration, and C−S stretch vibration.[37] These results confirm that the DDT and the OLA

https://doi.org/10.1021/acsanm.3c04490
ACS Appl. Nano Mater. 2023, 6, 22311−22319

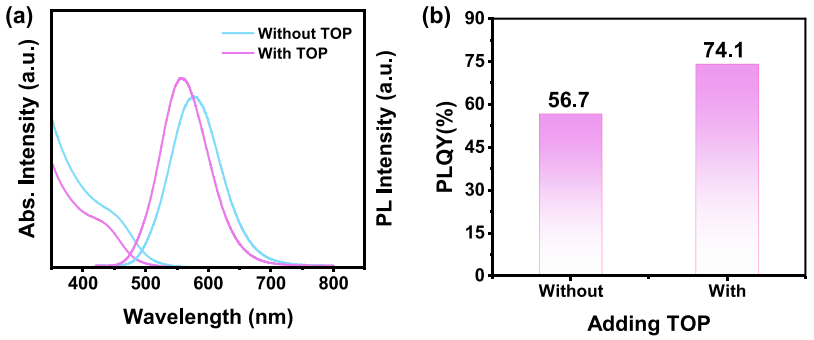

Figure 3. (a) UV−vis electronic absorption and PL spectra and (b) PLQY of AIS/ZS QDs without and with the TOP ligand.

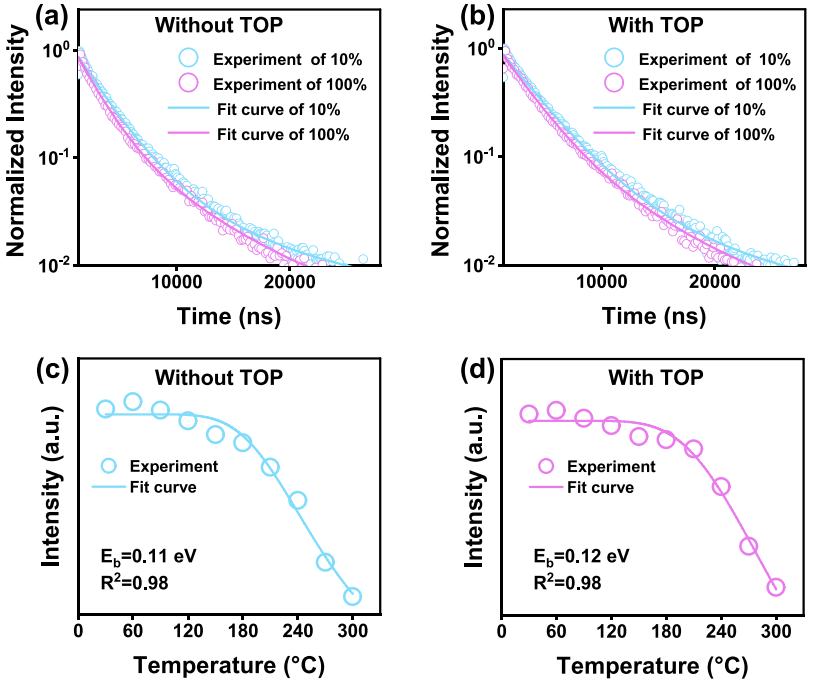

Figure 4. PL decay profiles of AIS/ZS QDs (a) without TOP and (b) with the TOP ligand measured at different excitation light energies. The laser light is transmitted through a filter with a transmittance of 10% or without a filter. Under a constant excitation light intensity, PL intensities of (c) without TOP and (d) with TOP ligand at temperatures ranging from 30 to 300 K. R^2 is the coefficient of determination.

ligands are bound to the surface of AIS/ZS QDs successfully. In addition, the S−H characteristic peak of 2557 cm^{-1} of DDT did not appear, which suggests that the S−H bond in DDT was cut off, and DDT was connected to the surface of QDs through the chemical bond formed between S and QDs. The AIS/ZS spectra show the characteristic features of TOP, including peaks in the 1000−1200 cm^{-1} region associated with C−P stretching vibration.[37] This indicates that TOP is bound to the surface of the AIS/ZS QDs. TOP is well-known to coordinate with chalcogens. In this work, we believe that TOP can effectively passivate the S-vacancy on the surface of QDs, forming a more stable tri-*n*-octylphosphine sulfide. It cooperates with DDT and the ligands of the OLA group to wrap the surface of quantum dots to form a stable dispersed system.

Figure 3a shows the UV−vis electronic absorption and emission spectra with or without the TOP ligand. After adding the TOP ligand, the excitonic absorption peak blue-shifts from 458 to 438 nm, while the PL peak shifts from 577 to 557 nm with a 410 nm excitation. The PLQY, as shown in Figure 3b, increased from 56.7 to 74.1% with TOP added, which is attributed to an effective passivation of surface defect sites related to S by TOP.[36]

Figure 4a,b and Figure S5a,b show the PL decay profiles and PL intensity of AIS/ZS QDs. Low energy lasers are represented in blue, and high energy lasers are represented in pink. With the energy of the excitation light increasing, the PL decays faster. After fitting the PL decay curve, the average lifetime τ^* is calculated

$$\tau^* = \frac{A_1\tau_1 + A_2\tau_2}{A_1 + A_2} \tag{6}$$

where parameters A_1, τ_1, A_2, and τ_2 were determined by fitting analysis; specific values are listed in Table S4. The τ_1 and τ_2 both show a decreasing trend with the increase of the excitation light energy. Moreover, the relative contribution rate of A_1/A_2 increases from 2.08 to 3.03 (without TOP) and from 1.48 to 1.72 (with TOP), respectively. Simultaneously, the τ^* decreases with the augmentation of excitation light energy from 2.04 to 1.68 μs (without TOP) and from 2.75 to 2.34 μs (with TOP). The photoluminescence mechanism of AIS/ZS QDs can be divided into a donor−acceptor pair (DAP)

https://doi.org/10.1021/acsanm.3c04490
ACS Appl. Nano Mater. 2023, 6, 22311−22319

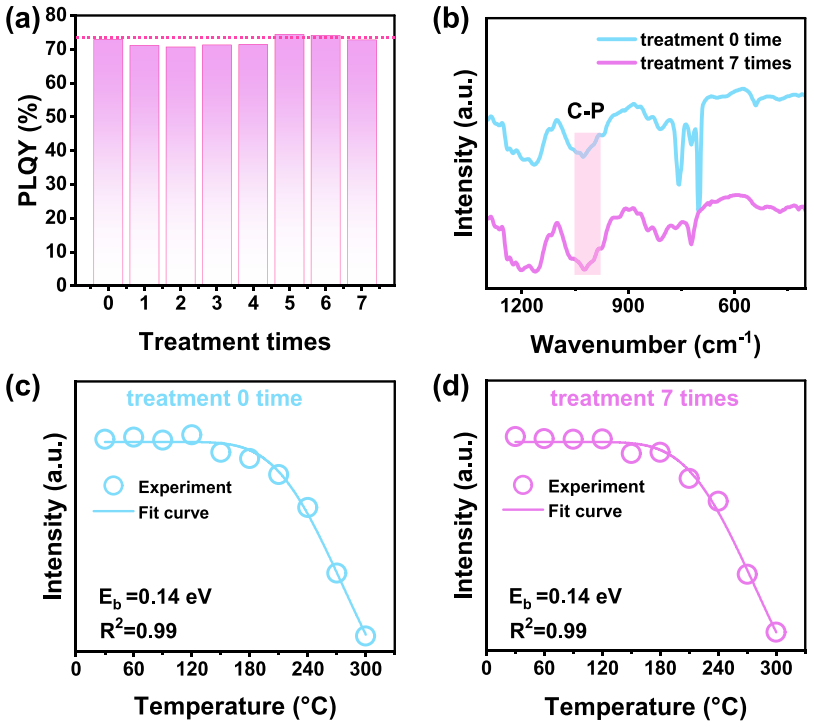

Figure 5. (a) PLQY histogram corresponding to treatment with polar solvent for 0−7 times. (b) FT-IR spectra of the AIS/ZS QDs for treatment with polar solvent 0 or 7 times. Under constant excitation light intensity, PL intensity of AIS/ZS QDs (c) without treatment with polar solvent and (d) treated with polar solvent 7 times at temperatures ranging from 30 to 300 K. R^2 is the coefficient of determination.

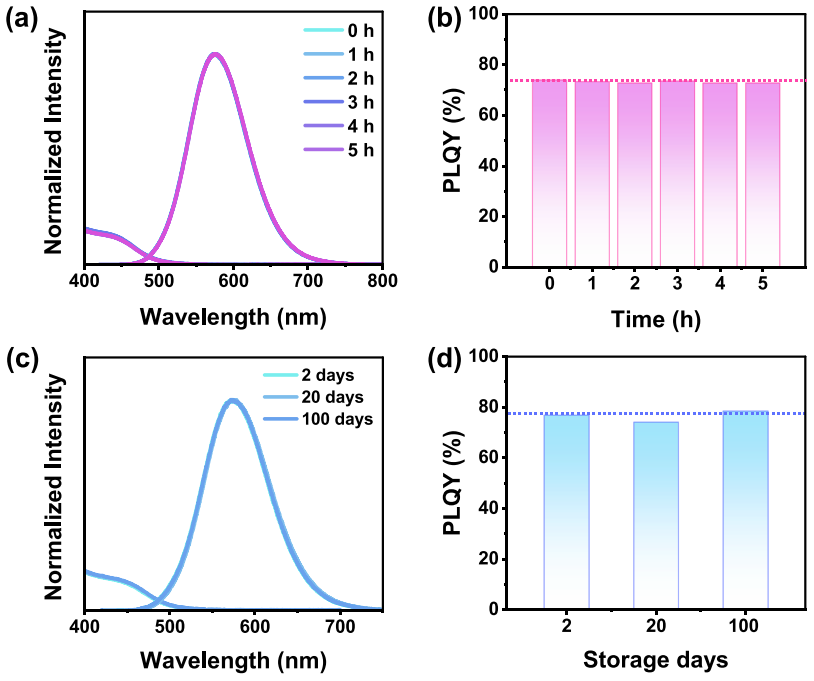

Figure 6. (a) Normalized electronic absorption and PL emission spectra of AIS/ZS QDs. (b) PLQY histogram corresponding to continuous laser irradiation for 5 h. (c) Normalized absorption and emission spectra. (d) PLQY histogram corresponding to storage for 100 days.

recombination and free-to-bond (FTB) recombination. For DAP recombination, with the increase of the excitation light energy, the DAP recombination probability increased and the PL decay time becomes shorter.[38] In this study, the average decay time decreases with an increase in the excitation energy, which is consistent with the DAP recombination mechanism. In the DAP recombination mechanism, the distant pairs have lower transition energies, while the closer pairs have higher transition energies. When the donor−acceptor on the surface of the QDs is passivated by TOP, the donor−acceptor is left behind. The average distance between the donor and acceptor in each QD decreases, causing the DAP emission peak to shift to the side with a higher energy.[39] We believe that this is the

https://doi.org/10.1021/acsanm.3c04490
ACS Appl. Nano Mater. 2023, 6, 22311−22319

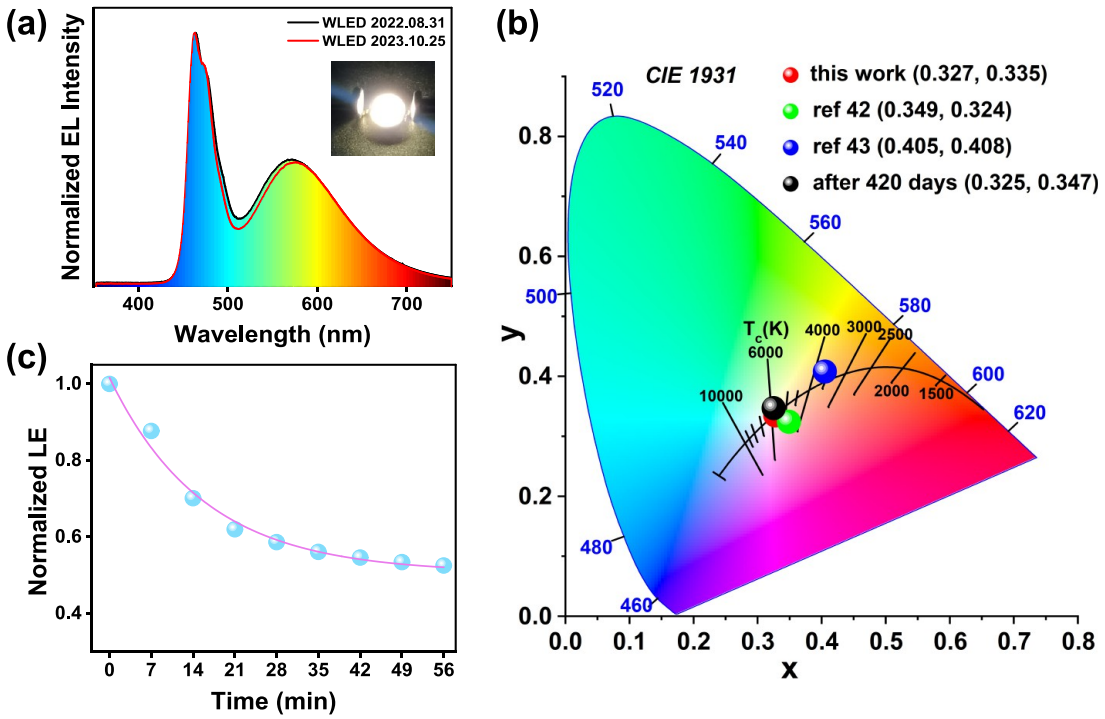

Figure 7. (a) emission spectrum of AIS/ZS QD-based white LED of 2022.08.31 and 2023.10.25 with the inset showing a photograph of the LED. (b) CIE coordinates of the white LED based on AIS/ZS QDs (red), the white LED reported (green[42] and blue[43]), and the white LED stored for 420 days (black). (c) Attenuation curve of the light efficiency over time.

reason for the blue shift in the PL peak position of QDs after TOP treatment.

The Arrhenius equation can be used to fit the integral strength of the variable-temperature PL peak

$$I(T) = \frac{I_0}{1 + Ae^{-E_b/k_B T}}$$

where I_0 and k_B are the PL intensity at 0 K and Boltzmann's constant, respectively. Figure S5c,d shows the PL intensity of the two types of samples measured under a constant excitation intensity within the temperature range of 30−300 K. With the increase of the temperature, the PL intensity gradually decreases and red-shifts, which can be attributed to the thermal quenching of DAP recombination pairs. Using the Arrhenius equation, we can know that, after adding the TOP ligand, the E_b was increased from 0.11 to 0.12 eV (Figure 4c,d). In the DAP recombination mechanism, the E_b of DAP is related to the Coulombic force of the donor−acceptor pair, and the Coulombic force is related to the distance between the donor and acceptor pair. The closer pairs have higher transition energies. The pairs with high transition energy have higher recombination probability and greater PLQY.[38] The TOP ligand can effectively increase E_b, increase the binding probability of DAP donor−acceptor recombination pairs, and ultimately lead to a higher PLQY.

2.3. Stability Analysis. Figure S6 shows the diluent AIS/ZS QDs in the sunlight corresponding to treatment with polar solvent for 0−7 times, the QDs repeatedly dissolved in *n*-hexane without any occurrence of aggregation. Comparing the normalized absorption and emission spectra (Figure S7), the spectra coincide perfectly. The PLQY fluctuates slightly (Figure 5a), maintaining between 70 and 74%. The FT-IR spectra of AIS/ZS QDs before and after treatment with polar solvent seven times are shown in Figure 5b. The two spectra are almost identical, and all maintain the characteristic peaks of TOP, which show that, after repeated treatment with polar solvent, the ligands are still on the surface of AIS/ZS QDs.

Figure 5c,d shows the PL intensity of AIS/ZS QDs at temperatures ranging from 30 to 300 k under a constant excitation light energy. After treatment for 0 or 7 times, both the values of E_b are equal to 0.14 eV. This means that, after repeated treatment with polar solvents, the surface ligands remain intact to protect the QDs, the DAP recombination pairs of AIS/ZS QDs are almost not reduced, and the radiation recombination probability remains at a high level. AIS/ZS QDs prepared by this method have excellent surface stability.

Figure 6a,b shows the electronic absorption and PL emission spectra and PLQY after 5 h of continuous UV laser irradiation (410 nm, 150 W); the spectra are normalized for different samples for comparison. The PL and absorption spectra remain unchanged with only a slight fluctuation for the PLQY between 73 and 74%, revealing excellent photostability. Moreover, the optical properties and PLQY are rather stable for the prepared QDs even storing for 100 days in a glass vial in air (Figure 6c,d). AIS/ZS QDs synthesized by this method still maintain the same PLQY and excellent dispersion after various conditions, which proves that the ligands binding in this preparation method are firmly bound to the surface of the QDs.

2.4. White LED Application. Due to the advantages of a high PLQY, tunable emission, a large Stokes shift, and being heavy metal-free, AIS/ZS QDs are ideal luminescent materials to prepare white LEDs.[40,41] At present, white LEDs are mainly prepared by mixing phosphors with QDs. Owing to the large particle size and poor dispersion of phosphor, it is more susceptible to scattering, reflection, and refraction. Here, we directly integrate AIS/ZS QDs with 460 nm blue chips and realize a white LED with a nearly pure white light emission.

https://doi.org/10.1021/acsanm.3c04490
ACS Appl. Nano Mater. 2023, 6, 22311−22319

The emission spectrum of the white LED driven at the current of 50 mA is shown in Figure 7a, and the inset of which shows the luminous photograph of the white LED. The luminous efficiency of the LED is 41.3 lm/W with a color temperature of 5734 K. As shown in Figure 7b, compared with the previously reported white LEDs based on AIS QDs,[42,43] the white LED prepared in this work shows the CIE coordinate of (0.327, 0.335), which is the closest one to pure white light of (0.33,0.33). We further investigated the stability of the prepared white LED. After 420 days of storage in the air, the EL spectrum of the unpackaged LED still maintained excellent stability, and its CIE coordinate changed from only (0.327, 0.335) to (0.325, 0.347) (Figure 7b). In order to accelerate device aging, we continuously drive the LED at a current of 10 mA. Figure 7c shows the attenuation curve of the light efficiency over time. Notably, after 56 min of continuous driving, the light efficiency of the LED can still maintain 52.5% of its initial value, indicating that the white LEDs prepared by our experimental method have great potential as a candidate for practical white light sources.

4. CONCLUSIONS

To summarize, we synthesized small-sized highly stable AIS/ZS QDs under low-temperature conditions without the need for inert gas protection with an average particle size of 1.73 ± 0.29 nm. As the reaction temperature increases from 60 to 210 °C, the first exciton absorption peak red shifts from 479 to 573 nm, while the emission peak red shifts from 548 to 666 nm with excitation at 410 nm. Surface passivation with the TOP increases the PLQY of the QDs to 74.1%. The AIS/ZS QDs exhibited outstanding stability under repeated treatment with polar solvents or prolonged laser irradiation, the QDs retained a high PLQY and good dispersion, which is attributed to strong passivation of the QDs by ligands. A DAP recombination mechanism is proposed for PL emission. Finally, integrating the AIS/ZS QDs onto a 460 nm LED chip resulted in an ideal white LED with a high luminous efficiency of 41.3 lm/W and CIE coordinates of (0.327, 0.335). This study demonstrates a facile preparation process for synthesizing highly stable AIS/ZS QDs with the potential for large-scale LEDs and biological applications.

5. EXPERIMENT

5.1. Materials. Indium triacetate ($In(C_2H_3O_2)_3$, 99.99%), oleylamine (OLA, 80−90%), 1-octadecene (ODE, 90%), 1-dodecanethiol (DDT, 98%), trioctylphosphine (TOP, 90%), and *n*-hexane (95%) were purchased from Aladdin. Silver acetate ($Ag(C_2H_3O_2)_3$, 99.5%), zinc acetate ($Zn(C_2H_3O_2)_2$, 99%), and ethanol (99.7%) were purchased from Macklin, and S (99.5%) was purchased from Tianjin Huadong Reagent. Glass glue, 460 nm chips, was purchased from Eucrystal Optoelectronics. All the materials were used without further purification.

5.2. Synthesis of AIS/ZS QDs. A thermal injection method was adopted to synthesize the AIS/ZS QDs. Using Ag:In = 1:5 as an example, S (0.200 mmol) and $Zn(C_2H_3O_2)_2$ (0.200 mmol) were dissolved in OLA (2.275 mM) as ZnS solution. First, raw materials, including $In(C_2H_3O_2)_3$ (0.125 mmol), $Ag(C_2H_3O_2)_3$ (0.025 mmol), OLA (0.91 mM), TOP (0.09 mM), and ODE (18.8 mM), were loaded into a three-neck flask and then DDT (2.00 mM) was injected in the solution under intense stirring at the temperature of 60 °C. After stirring for 10 min, the S source prepared by dissolving 0.200 mmol of S in 1.03 mM of OLA was injected into the above solution, and the temperature was rapidly raised to 90 °C. After stirring and reacting for another 10 min, the ZnS solution was gradually added to the flask, and another 10 min reaction was needed to complete the synthesis of AIS/ZS QDs. The final solution was cooled with ice water to reduce the temperature. We mixed the final solution with ethanol solution (5.14 mol) and centrifuged twice for 10 min at a speed of 8800 rpm/s. Finally, the precipitate of AIS/ZS QDs was dissolved in *n*-hexane (23 mM) for further study. A volume of 20 μL/mL TOP was added into the *n*-hexane to further enhance the stability of the final products.

5.3. Treatment with Polar Solvent. The AIS/ZS QDs were treated with ethanol. The ratio of ethanol/QD solution was 1:30. After being mixed thoroughly and allowed to stand briefly, the mixture was centrifuged. The resulting solid sample was left to stand for 1 h. It was then fully dissolved using 3.00 mL of *n*-hexane. Subsequently, the process was continued by treating the sample with ethanol in a 30-fold volume. This entire procedure was repeated for a total of 7 cycles. The surface modification of organic ligands can passivate the surface defects of semiconductor NPs and improve the luminescence performance. However, the ligand is not bound to the surface of the NPs firmly. The binding ability of surface ligands to QDs can be obtained using polar solvents for multiple treatments.

5.4. Preparation of White LEDs with AIS/ZS QDs. AIS/ZS QDs solution (0.0500 mL) with a concentration of 40 mg/mL was fully mixed with 0.2 g of glass glue. Then, the above mixture (0.0500 g) was evenly coated on the chip with a light wavelength of 460 nm. After natural drying in air, the white LEDs were obtained.

5.5. Characterization. A UV-3101 spectrophotometer and HitachiF-7000 fluorescence spectrometer were employed to measure the electronic absorption (Abs) and photoluminescence (PL) spectra of QDs, respectively. An FEI Tecnai F20 transmission electron microscope (TEM) was used to analyze the sample morphology and size. Malvern Zetasizer NanoZS was used to measure the dynamic spectral scattering data and analyze the particle size. Genesis 2000 energy-dispersive X-ray spectroscopy (EDXA) was used to analyze the elemental composition of samples. The fluorescence lifetime was measured with an Edinburgh FLS920 fluorescence spectrometer. In the measurement of temperature-dependent time-resolved PL (TPRL), the 400 nm pulse laser with a 10 ns duration of a Surelite II-10 pumped Horizon OPO was used as the excitation source, and the signal was detected using an R9110 PMT TCSPC (Hamamatsu, Japan) and recorded by a TDS3052B Oscilloscope. Fourier transform infrared (FT-IR) spectra were measured using a VERTEX 70 V spectrometer. The PLQY was obtained by a comparison method with the reference sample of rhodamine 6G. The emission spectrum of the white LED was measured by an integrating sphere (HAAS-2000). The photos under UV light were taken by a mobile phone.

■ ASSOCIATED CONTENT

Supporting Information

The Supporting Information is available free of charge at https://pubs.acs.org/doi/10.1021/acsanm.3c04490.

https://doi.org/10.1021/acsanm.3c04490
ACS Appl. Nano Mater. 2023, 6, 22311−22319

Absorption, PL and exciton absorption spectra of AIS/ZS QDs, particle size histogram, time-resolved PL, temperature-dependent time-resolved PL, photograph and normalized absorption-PL spectra of AIS/ZS QDs after 0−7 times of treatment, fluorescence lifetimes, k_{nr} and k_r, elemental compositions, and PL decay curve data of AIS/ZS QDs (PDF)

AUTHOR INFORMATION

Corresponding Authors

Ying Lv − *State Key Laboratory of Luminescence and Applications, Changchun Institute of Optics, Fine Mechanics and Physics, Chinese Academy of Sciences, Changchun 130033, China;* orcid.org/0000-0003-1649-5258; Phone: +86-431-86176341; Email: lvying@ciomp.ac.cn

Qinghui Zeng − *Changchun University of Chinese Medicine, Changchun 130017, China;* orcid.org/0000-0002-1211-3980; Email: zengqinghui96000@163.com

Wenyu Ji − *College of Physics, Jilin University, Changchun 130012, China;* orcid.org/0000-0003-2932-5119; Email: jiwy@jlu.edu.cn

Authors

Yifang Sun − *State Key Laboratory of Luminescence and Applications, Changchun Institute of Optics, Fine Mechanics and Physics, Chinese Academy of Sciences, Changchun 130033, China; University of Chinese Academy of Sciences, Beijing 100049, China;* orcid.org/0009-0006-1518-617X

Liangliang Zhang − *State Key Laboratory of Luminescence and Applications, Changchun Institute of Optics, Fine Mechanics and Physics, Chinese Academy of Sciences, Changchun 130033, China;* orcid.org/0000-0002-9546-8786

Xiaoyang Guo − *State Key Laboratory of Luminescence and Applications, Changchun Institute of Optics, Fine Mechanics and Physics, Chinese Academy of Sciences, Changchun 130033, China;* orcid.org/0000-0003-0259-137X

Xingyuan Liu − *State Key Laboratory of Luminescence and Applications, Changchun Institute of Optics, Fine Mechanics and Physics, Chinese Academy of Sciences, Changchun 130033, China;* orcid.org/0000-0002-9681-1646

Complete contact information is available at: https://pubs.acs.org/10.1021/acsanm.3c04490

Notes

The authors declare no competing financial interest.

ACKNOWLEDGMENTS

This work is supported by the National Natural Science Foundation of China (nos. 62035013, 51973208, 61875195, 61975256, and 62175235), the Jilin Scientific and Technological Development Program (no. 20220201064GX and 20180201057YY), the Youth Innovation Promotion Association of the Chinese Academy of Sciences (no. 2019225), and the Project supported by the Dawn Talent Training Program of CIOMP.

REFERENCES

(1) Alivisatos, A. P. Semiconductor clusters, nanocrystals, and quantum dots. *Science* **1996**, *271* (5251), 933−937.

(2) Abe, S.; Joos, J. J.; Martin, L. I.; Hens, Z.; Smet, P. F. Hybrid remote quantum dot/powder phosphor designs for display backlights. *Light Sci. Appl.* **2017**, *6* (6), No. e16271.

(3) Mittelstädt, A.; Schliwa, A.; Klenovský, P. Modeling electronic and optical properties of III−V quantum dots—selected recent developments. *Light Sci. Appl.* **2022**, *11* (1), 17.

(4) Kelleher, B.; Dillane, M.; Viktorov, E. A. Optical information processing using dual state quantum dot lasers: complexity through simplicity. *Light Sci. Appl.* **2021**, *10* (1), 238.

(5) Hu, X.; Xu, Y.; Wang, J.; Ma, J.; Wang, L.; Jiang, W. In Situ Fabrication of Superfine Perovskite Composite Nanofibers with Ultrahigh Stability by One-Step Electrospinning Toward White Light-Emitting Diode. *Adv. Fiber Mater.* **2023**, *5* (1), 183−197.

(6) Grillot, F.; Duan, J.; Dong, B.; Huang, H. Uncovering recent progress in nanostructured light-emitters for information and communication technologies. *Light Sci. Appl.* **2021**, *10* (1), 156.

(7) Zhu, X.; Bian, L.; Fu, H.; Wang, L.; Zou, B.; Dai, Q.; Zhang, J.; Zhong, H. Broadband perovskite quantum dot spectrometer beyond human visual resolution. *Light Sci. Appl.* **2020**, *9*, 73.

(8) Klimov, V. I. Optical nonlinearities and ultrafast carrier dynamics in semiconductor nanocrystals. *J. Phys. Chem. B* **2000**, *104* (26), 6112−6123.

(9) Ko, M.; Yoon, H. C.; Yoo, H.; Oh, J. H.; Yang, H.; Do, Y. R. Highly Efficient Green Zn-Ag-In-S/Zn-In-S/ZnS QDs by a Strong Exothermic Reaction for Down-Converted Green and Tripackage White LEDs. *Adv. Funct. Mater.* **2017**, *27* (4), 1602638.

(10) Kovalenko, M. V.; Protesescu, L.; Bodnarchuk, M. I. Properties and potential optoelectronic applications of lead halide perovskite nanocrystals. *Science* **2017**, *358* (6364), 745−750.

(11) Zhong, H. Z.; Bai, Z. L.; Zou, B. S. Tuning the Luminescence Properties of Colloidal I-III-VI Semiconductor Nanocrystals for Optoelectronics and Biotechnology Applications. *J. Phys. Chem. Lett.* **2012**, *3* (21), 3167−3175.

(12) Aldakov, D.; Lefrancois, A.; Reiss, P. Ternary and quaternary metal chalcogenide nanocrystals: synthesis, properties and applications. *J. Mater. Chem. C* **2013**, *1* (24), 3756−3776.

(13) Baimuratov, A. S.; Martynenko, I. V.; Baranov, A. V.; Fedorov, A. V.; Rukhlenko, I. D.; Kruchinin, S. Y. Giant Stokes Shifts in $AgInS_2$ Nanocrystals with Trapped Charge Carriers. *J. Phys. Chem. C* **2019**, *123* (26), 16430−16438.

(14) Kameyama, T.; Takahashi, T.; Machida, T.; Kamiya, Y.; Yamamoto, T.; Kuwabata, S.; Torimoto, T. Controlling the Electronic Energy Structure of ZnS-$AgInS_2$ Solid Solution Nanocrystals for Photoluminescence and Photocatalytic Hydrogen Evolution. *J. Phys. Chem. C* **2015**, *119* (44), 24740−24749.

(15) Delices, A.; Moodelly, D.; Hurot, C.; Hou, Y. X.; Ling, W. L.; Saint-Pierre, C.; Gasparutto, D.; Nogues, G.; Reiss, P.; Kheng, K. Aqueous Synthesis of DNA-Functionalized Near-Infrared $AgInS_2$/ZnS Core/Shell Quantum Dots. *ACS Appl. Mater. Inter* **2020**, *12* (39), 44026−44038.

(16) Pilch, J.; Matysiak-Brynda, E.; Kowalczyk, A.; Bujak, P.; Mazerska, Z.; Nowicka, A. M.; Augustin, E. New Unsymmetrical Bisacridine Derivatives Noncovalently Attached to Quaternary Quantum Dots Improve Cancer Therapy by Enhancing Cytotoxicity toward Cancer Cells and Protecting Normal Cells. *ACS Appl. Mater. Inter* **2020**, *12* (15), 17276−17289.

(17) Vitshima, N. A.; Silwana, B.; Tsolekile, N.; Matoetoe, M. C. Effect of ZnS coating on the optoelectronic properties of aqueous glutathione capped AgInS quantum dots. *J. Alloys Compd.* **2022**, *900*, 163386.

(18) Subramaniam, P.; Lee, S. J.; Shah, S.; Patel, S.; Starovoytov, V.; Lee, K. B. Generation of a Library of Non-Toxic Quantum Dots for Cellular Imaging and siRNA Delivery. *Adv. Mater.* **2012**, *24* (29), 4014−4019.

(19) Dhamo, L.; Carulli, F.; Nickl, P.; Wegner, K. D.; Hodoroaba, V. D.; Würth, C.; Brovelli, S.; Resch-Genger, U. Efficient Luminescent Solar Concentrators Based on Environmentally Friendly Cd-Free Ternary AIS/ZnS Quantum Dots. *Adv. Opt. Mater.* **2021**, *9* (17), 2100587.

(20) Yang, D.; Wei, X.; Piao, Z.; Cui, Z.; He, H.; Wen, Z.; Zhang, W.; Wang, L.; Mei, S.; Guo, R. Constructing bimodal nanoprobe based on Gd:$AgInS_2$/ZnS quantum dots for fluorometric/magnetic resonance imaging in mesenchymal stem cells. *J. Mater. Sci. Technol.* **2023**, *148*, 116−122.
(21) Du, J.; Ma, S.; Liu, H.; Fu, H.; Li, L.; Li, Z.; Li, Y.; Zhou, J. Uncovering the mechanism of novel $AgInS_2$ nanosheets/TiO_2 nanobelts composites for photocatalytic remediation of combined pollution. *Appl. Catal. B Environ* **2019**, *259*, 118062.
(22) Cai, Q.; Yin, T.; Ye, Y.; Jie, G.; Zhou, H. Versatile Photoelectrochemical Biosensing for Hg^{2+} and Aflatoxin B1 Based on Enhanced Photocurrent of $AgInS_2$ Quantum Dot-DNA Nanowires Sensitizing NPC-ZnO Nanopolyhedra. *Anal. Chem.* **2022**, *94* (15), 5814−5822.
(23) Huang, X.; Huang, Y.; Yan, F.; Xue, X.; Zhang, K.; Cai, P.; Zhang, X.; Zhang, X. Constructing defect-related subband in silver indium sulfide QDs via pH-dependent oriented aggregation for boosting photocatalytic hydrogen evolution. *J. Colloid Interface Sci.* **2021**, *593*, 222−230.
(24) Wang, K.; Qin, H.; Li, J.; Cheng, Q.; Zhu, Y.; Hu, H.; Peng, J.; Chen, S.; Wang, G.; Chou, S.; Dou, S.; Xiao, Y. Metallic $AgInS_2$ nanocrystals with sulfur vacancies boost atmospheric CO_2 photoreduction under near-infrared light illumination. *Appl. Catal. B Environ* **2023**, *332*, 122763.
(25) Juneja, R.; Singh, A. K. Rattling-Induced Ultralow Thermal Conductivity Leading to Exceptional Thermoelectric Performance in $AgIn_5S_8$. *ACS Appl. Mater. Inter* **2019**, *11* (37), 33894−33900.
(26) Torimoto, T.; Adachi, T.; Okazaki, K.-I.; Sakuraoka, M.; Shibayama, T.; Ohtani, B.; Kudo, A.; Kuwabata, S. Facile synthesis of ZnS-$AgInS_2$ solid solution nanoparticles for a color-adjustable luminophore. *J. Am. Chem. Soc.* **2007**, *129* (41), 12388.
(27) Dai, M. L.; Ogawa, S.; Kameyama, T.; Okazaki, K.; Kudo, A.; Kuwabata, S.; Tsuboi, Y.; Torimoto, T. Tunable photoluminescence from the visible to near-infrared wavelength region of non-stoichiometric $AgInS_2$ nanoparticles. *J. Mater. Chem.* **2012**, *22* (25), 12851−12858.
(28) Liu, L. W.; Hu, R.; Law, W. C.; Roy, I.; Zhu, J.; Ye, L.; Hu, S. Y.; Zhang, X. H.; Yong, K. T. Optimizing the synthesis of red- and near-infrared $CuInS_2$ and $AgInS_2$ semiconductor nanocrystals for bioimaging. *Analyst* **2013**, *138* (20), 6144−6153.
(29) Chen, T.; Hu, X. B.; Xu, Y. Q.; Wang, L. J.; Jiang, W. H.; Jiang, W.; Xie, Z. X. Hydrothermal synthesis of highly fluorescent Ag-In-S/ZnS core/shell quantum dots for white light-emitting diodes. *J. Alloys Compd.* **2019**, *804*, 119−127.
(30) Ma, H. T.; Pan, L. J.; Wang, J.; Zhang, L.; Zhang, Z. L. Synthesis of $AgInS_2$ QDs in droplet microreactors: Online fluorescence regulating through temperature control. *Chin. Chem. Lett.* **2019**, *30* (1), 79−82.
(31) Jin, X.; Xie, K.; Zhang, T.; Lian, H.; Zhang, Z.; Xu, B.; Li, D.; Li, Q. Cation exchange assisted synthesis of ZnCdSe/ZnSe quantum dots with narrow emission line widths and near-unity photoluminescence quantum yields. *Chem. Commun.* **2020**, *56* (45), 6130−6133.
(32) Kwon, H.; Lee, T.; Kim, K.; Kim, D.; Seo, H.; Kwon, O.; Kwak, J.; Kim, S. Enhanced Stability and Highly Bright Electroluminescence of AgInZnS/CdS/ZnS Quantum Dots through Complete Isolation of Core and Shell via a CdS Interlayer. *Small* **2023**, 2304592.
(33) Han, N. S.; Yoon, H. C.; Jeong, S.; Oh, J. H.; Park, S. M.; Do, Y. R.; Song, J. K. Origin of highly efficient photoluminescence in $AgIn_5S_8$ nanoparticles. *Nanoscale* **2017**, *9* (29), 10285−10291.
(34) Xu, Y.; Chen, T.; Xie, Z.; Jiang, W.; Wang, L.; Jiang, W.; Zhang, X. Highly efficient Cu-In-Zn-S/ZnS/PVP composites based white light-emitting diodes by surface modulation. *Chem. Eng. J.* **2021**, *403*, 126372.
(35) Chang, J. Y.; Wang, G. Q.; Cheng, C. Y.; Lin, W. X.; Hsu, J. C. Strategies for photoluminescence enhancement of $AgInS_2$ quantum dots and their application as bioimaging probes. *J. Mater. Chem.* **2012**, *22* (21), 10609−10618.
(36) Qasrawi, A. F. Annealing effects on the structural and optical properties of $AgIn_5S_8$ thin films. *J. Alloys Compd.* **2008**, *455* (1−2), 295−297.
(37) Pal, N. K.; Kryschi, C. A facile one-pot synthesis of blue and red luminescent thiol stabilized gold nanoclusters: a thorough optical and microscopy study. *Phys. Chem. Chem. Phys.* **2015**, *17* (33), 21423−21431.
(38) Ogawa, T.; Kuzuya, T.; Hamanaka, Y.; Sumiyama, K. Synthesis of Ag−In binary sulfide nanoparticles—structural tuning and their photoluminescence properties. *J. Mater. Chem.* **2010**, *20* (11), 2226−2231.
(39) Hirase, A.; Hamanaka, Y.; Kuzuya, T. Ligand-Induced Luminescence Transformation in $AgInS_2$ Nanoparticles: From Defect Emission to Band-Edge Emission. *J. Phys. Chem. Lett.* **2020**, *11* (10), 3969−3974.
(40) Lin, H.; Yang, J.; Liu, Y.-f.; Zeng, F.-j.; Tang, X.-S.; Yao, Z.-q.; Guan, H.-l.; Xiong, Q.; Zhou, J.-e.; Wu, D.-f.; Du, J. Stable and efficient hybrid Ag-In-S/ZnS@SiO_2-carbon quantum dots nanocomposites for white light-emitting diodes. *Chem. Eng. J.* **2020**, *393*, 124654.
(41) Chen, Y.; Chen, T.; Qin, Z.; Xie, Z.; Liang, M.; Li, Y.; Lin, J. Rapid synthesis of $AgInS_2$ quantum dots by microwave assisted-hydrothermal method and its application in white light emitting diodes. *J. Alloys Compd.* **2023**, *930*, 167389.
(42) Su, D.; Wang, L.; Li, M.; Mei, S.; Wei, X.; Dai, H.; Hu, Z.; Xie, F.; Guo, R. Highly luminescent water-soluble $AgInS_2$/ZnS quantum dots-hydrogel composites for warm white LEDs. *J. Alloys Compd.* **2020**, *824*, 153896.
(43) Fang, Z.; Huang, Y.; Cheng, S.; Zhu, Q.; Zhang, W.; Zhao, F.; Huang, G.; Jiang, G.; Li, F. Quaternary alloyed quantum dots with a wide-ranging tunable emission for high color-rendering white light-emitting diodes. *J. Alloys Compd.* **2023**, *932*, 167608.

https://doi.org/10.1021/acsanm.3c04490
ACS Appl. Nano Mater. 2023, 6, 22311−22319